THE ASTRONOMICAL JOURNAL, 118:972–982, 1999 August

L1551 NE OR L1551 IRS 5: WHICH SOURCE DRIVES HH 28/29?

DAVID DEVINE
Laboratory for Astronomy and Solar Physics, NASA Goddard Space Flight Center, Code 681, Greenbelt, MD 20771
AND
BO REIPURTH AND JOHN BALLY
Center for Astrophysics and Space Astronomy, University of Colorado, Campus Box 389, Boulder, CO 80309
Received 1999 April 20; accepted 1999 April 26

ABSTRACT

We have obtained deep high-resolution interference filter images of the HH objects in the L1551 molecular cloud in 1990 and 1997, and we suggest that the well-known and well-studied objects HH 28 and 29 are driven by the deeply embedded class 0 source L1551 NE, not by the well-known IRS 5 source. We find a new, small bipolar HH flow, HH 454, surrounding L1551 NE. This new HH flow is aligned along the axis of a highly collimated infrared jet from this source, is blueshifted by 110 km s^{-1} southwest of the source, and is redshifted by 100–130 km s^{-1} northeast of L1551 NE. A line through the L1551 NE source and along this well-defined flow axis passes straight through HH 29 and within parts of the more distant HH 259 and HH 28. The proper motion of HH 29 exhibits a complex flow pattern with some knots appearing to move away from the nearby source IRS 5 while other parts are moving away from L1551 NE. The HH 29 object encompasses several bright, stationary knots that have faded between the two epoch images. When these stationary knots are excluded from the proper-motion analysis, the resulting overall flow vector points away from L1551 NE, not from IRS 5. Most components of HH 259 and some parts of HH 28 also appear to be moving in a direction pointing away from L1551 NE rather than from IRS 5. In the opposite, redshifted lobe, we find a new, distant HH object, HH 286, but it is unclear whether L1551 NE or IRS 5 is the driving source. Altogether, it appears that L1551 NE plays a much more prominent role than hitherto anticipated in the outflow activity of this highly complex and confused region.

Key words: ISM: jets and outflows — stars: formation — stars: mass loss

1. INTRODUCTION

The L1551 dark cloud, cataloged by Lynds (1962), is one of the nearest, best-known, and most-studied regions of low-mass star formation. Following the discovery of HH 28 and 29 in L1551 by Herbig (1974), an infrared survey of the cloud by Strom, Strom, & Vrba (1976) uncovered the now well-known embedded source IRS 5. Cudworth & Herbig (1979) noted high proper motions of HH 28/29 with vectors pointing away from the general direction of IRS 5, and Snell, Loren, & Plambeck (1980) found a large bipolar molecular outflow from IRS 5, with HH 28/29 inside its blue lobe. Since then an enormous literature has been built up on IRS 5 (for a list of references see Reipurth 1999[1]).

Emerson et al. (1984) discovered a second embedded source in L1551, called L1551 NE (hereafter NE), located only 149″ east-northeast of IRS 5. A faint, optical reflection nebula from NE was found by Draper, Warren-Smith, & Scarrott (1985) and Campbell et al. (1988), and a large, bright, infrared reflection nebula was imaged by Hodapp (1994). Faint redshifted Herbig-Haro objects (HH 262) were found in what appears to be the receding lobe of NE by Rodríguez et al. (1989), Graham & Heyer (1990), and Graham & Rubin (1992). NE was detected in the radio continuum at 3.5 cm by Rodríguez, Anglada, & Raga (1995), with tentative evidence that it is a binary with 0.″8 separation. Because NE is located toward the red lobe of the large IRS 5 flow, it is difficult to establish whether it has its own molecular outflow, but Moriarty-Schieven, Butner, & Wannier (1995) suggest the presence of a weak east-west oriented molecular flow from NE.

IRS 5 is a class I source, bright in the near-infrared and with a well-developed molecular flow. Light escaping from IRS 5 along the cavity excavated by the outflow illuminates a large reflection nebula (e.g., Stocke et al. 1988; Davis et al. 1995). In contrast to this, the reflection nebula associated with NE is relatively faint; hence, NE may be more deeply embedded than IRS 5 and is likely to be a class 0 source (e.g., Barsony & Chandler 1993). If we adopt a distance of 140 pc to the Taurus cloud (Kenyon, Dobrzycka, & Hartmann 1994), NE has a bolometric luminosity of only 4.5 $L_\odot$ (Emerson et al. 1984).

Figures 1 and 2 show the sum and difference of our KPNO 4 m MOSAIC Hα and [S II] images of the L1551 region. The complex emission that has been associated with the IRS 5 outflow is most likely due to the presence of multiple overlapping flows driven by IRS 5, NE, and young stars in the HL-Tau region; a more thorough discussion of the outflows in L1551 will be presented in a future paper (Bally et al. 2000). Reipurth et al. (1999) have detected a highly collimated infrared jet in [Fe II] emission emanating from NE using NICMOS at the *Hubble Space Telescope* (*HST*). In this paper we present evidence for a collimated HH flow from NE along the same axis as the [Fe II] jet, and we argue that the well-known objects HH 28 and 29 are most probably not driven by IRS 5, but rather are bright bow shocks in a highly collimated flow from NE.

2. OBSERVATIONS

High-resolution images of the region to the southwest of L1551 IRS 5 were obtained on the night of 1990

[1] Available at http://casa.colorado.edu/hhcat.

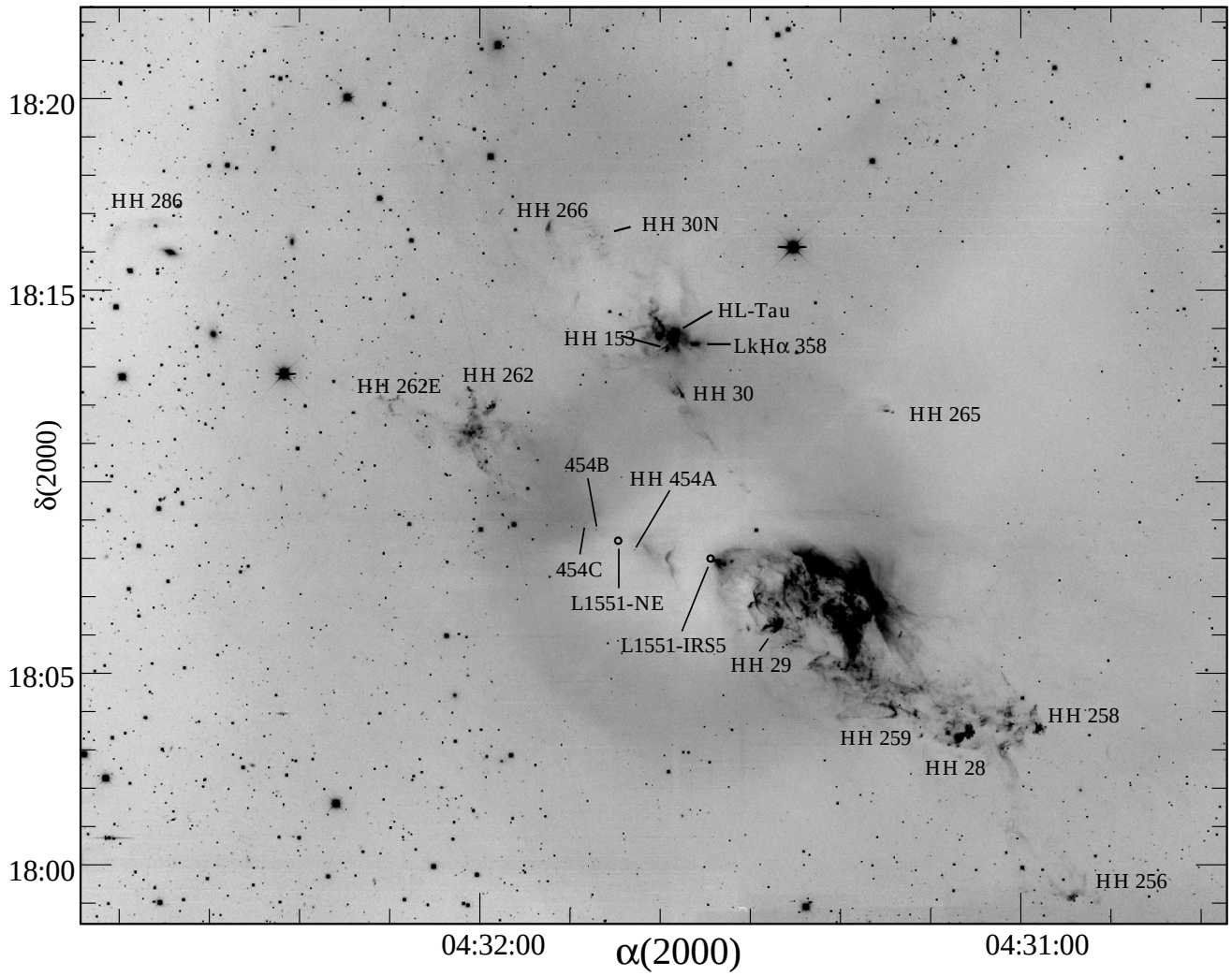

FIG. 1.—Wide-field KPNO MOSAIC image showing the Hα + [S II] emission in the L1551 region. The newly discovered HH 454 and HH 286 knots are shown, as well as several previously known HH objects. The complex nature of the line emission in this region is due to the presence of several overlapping HH flows driven by several very young sources.

November 22 with the ESO 3.5 m New Technology Telescope (NTT) and EMMI using a Thompson 1024 × 1024 pixel chip with a scale of 0.″439 pixel^{-1} and a resulting field of view of approximately 7.′5 × 7.′5. Single 30 minute exposures were obtained through an [S II] filter centered at 6728 Å and an FWHM of 74 Å (6728/74) and an Hα filter (6560/33). A single 5 minute continuum observation was obtained through a broadband Gunn z filter, which excludes all strong HH emission. The images were then reduced in the standard fashion within IRAF using sky flats obtained earlier in the evening. Cosmic rays were removed with the cosmic rays package in IRAF, and any remaining cosmic rays, chip defects, and bleeding effects were removed by hand.

We also obtained images of the L1551 region on the nights of 1997 October 29–31 at the prime focus of the Mayall 4 m telescope using the engineering-grade MOSAIC 8192 × 8192 detector. The field of view with the imaging correctors is approximately 36′ × 36′ with 0.″26 pixel^{-1}. In order to minimize the effects of bad columns and pixels, we obtained dithered sets of five 600 s exposures through narrowband filters transmitting Hα and [S II]. The Hα filter is centered on 6563 Å with a bandpass of 75 Å, while the [S II] filter is centered on 6723 Å with a bandpass of 80 Å. The data were overscanned, trimmed, dark subtracted, and then flat-fielded (using sky flats) in the standard manner, and the individual subframes were then combined into a single FITS image using the IRAF packages MSCZERO, MSCWCS, MSCIMAGE, and MSCSTACK following the guidelines set forth by Armandroff et al. (1999).[2] A central reflection persisted even after flat-fielding and median combining; this is a result of a defective antireflection coating on the corrective optics employed at the 4 m telescope in combination with the use of narrowband filters. The amount of reflection depends critically on the presence of bright stars near the imaging field and can vary between dithered images. The reflection is less noticeable in regions with high background emission.

We obtained moderate-resolution ($R \approx 6000$) spectra of HH 286 and HH 454 on the nights of 1996 January 8 and 1998 December 28, respectively. All spectra were obtained at the Mayall 4 m telescope at KPNO using a 2″ × 5′ slit on the Ritchey-Chrétien spectrograph with grating KPC24

[2] See http://www.noao.edu/kpno/mosaic/manual.

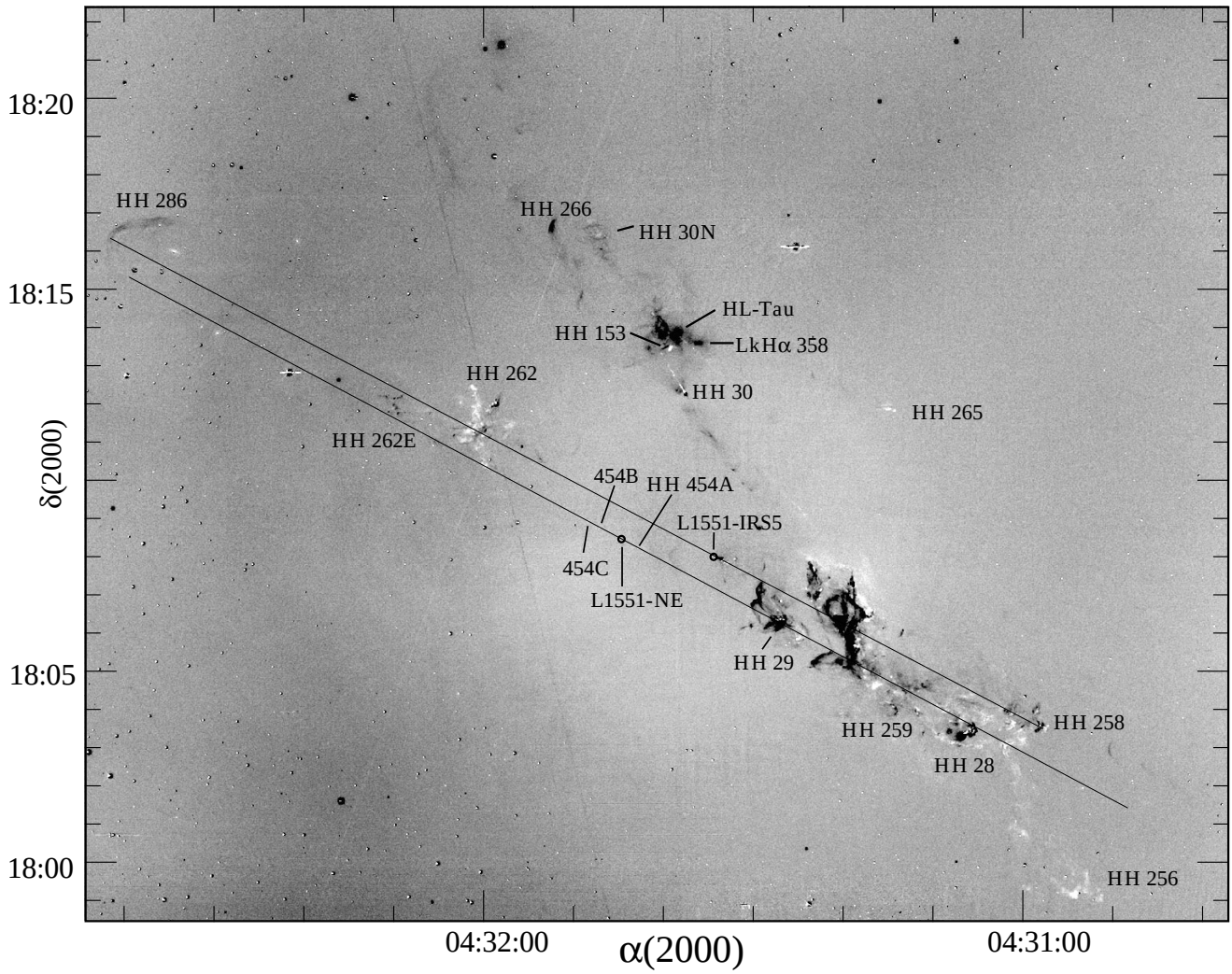

FIG. 2.—Difference between the Hα (*black*) and [S II] (*white*) KPNO MOSAIC images of the L1551 region. As discussed in the text, the alignment of the HH 454, HH 29, and HH 28 knots suggests a common origin in L1551 NE. A new counter bow shock, HH 286, may originate in either NE or IRS 5.

operating in the second order and a 2K × 2K CCD (T2KB). This arrangement gave a pixel scale of 0.54 Å in the red near Hα, which corresponds to a velocity resolution of about 24 km s^{-1} $pixel^{-1}$. The scale along the slit was 0″.6 $pixel^{-1}$. We used a quartz lamp to obtain flat fields and an HeNeAr comparison lamp for wavelength calibration. Our spectra covered the wavelength range from [O I] λ6300 to [S II] λ6731. The spectra were reduced following the procedures for reduction of long-slit spectra outlined by Massey, Valdes, & Barnes (1992).[3]

3. DISCUSSION

3.1. *The HH 454 Flow and HH 28/29*

Figure 3 shows an [S II] CCD image of the region around NE, with the VLA[4] position marked. Three knots are seen lying on a well-defined line through the VLA source. These knots are much brighter in [S II] than in Hα and make up a new HH flow, which we here call HH 454. The two sides of the flow are asymmetric, with the single knot A in the west-southwest lobe at a distance of 28″ from the source, while the east-northeast lobe contains the two knots B and C, which are located approximately 39″ and 63″ from the source. Our long-slit spectra show that HH 454A is blueshifted with a radial velocity of about −110 km s^{-1} relative to NE (which we assume has the velocity of the ambient cloud), that HH 454B is redshifted with $v = +100$ km s^{-1}, and that HH 454C is also redshifted with $v = 130$ km s^{-1}. All three knots exhibit relatively narrow [S II] line widths with $\Delta v < 40$ km s^{-1}. Additionally, a large low surface brightness reflection nebula is seen, which appears to have changed in appearance since the early broadband images of Draper et al. (1985).

It has always been assumed that the nearby objects HH 28 and 29 are powered by IRS 5. We here question this assumption and suggest that NE is a far more likely driving source. This is based on the following observational facts:

1. The position angle of the well-aligned knots in the HH 454 flow is within 2° of the axis of the highly collimated infrared [Fe II] jet found by Reipurth et al. (1999), thus forming a very well defined line through the NE source. When this line is extended to the southwest, it passes precisely through HH 29, which is 5′ away and deviates by only 3° from a line drawn between NE and HH 28, which is more

[3] Electronically available at http://iraf.noao.edu/docs/spectra.html.

[4] The VLA is a telescope of the National Radio Astronomy Observatory, which is operated by Associated Universities, Inc., under a cooperative agreement with the National Science Foundation.

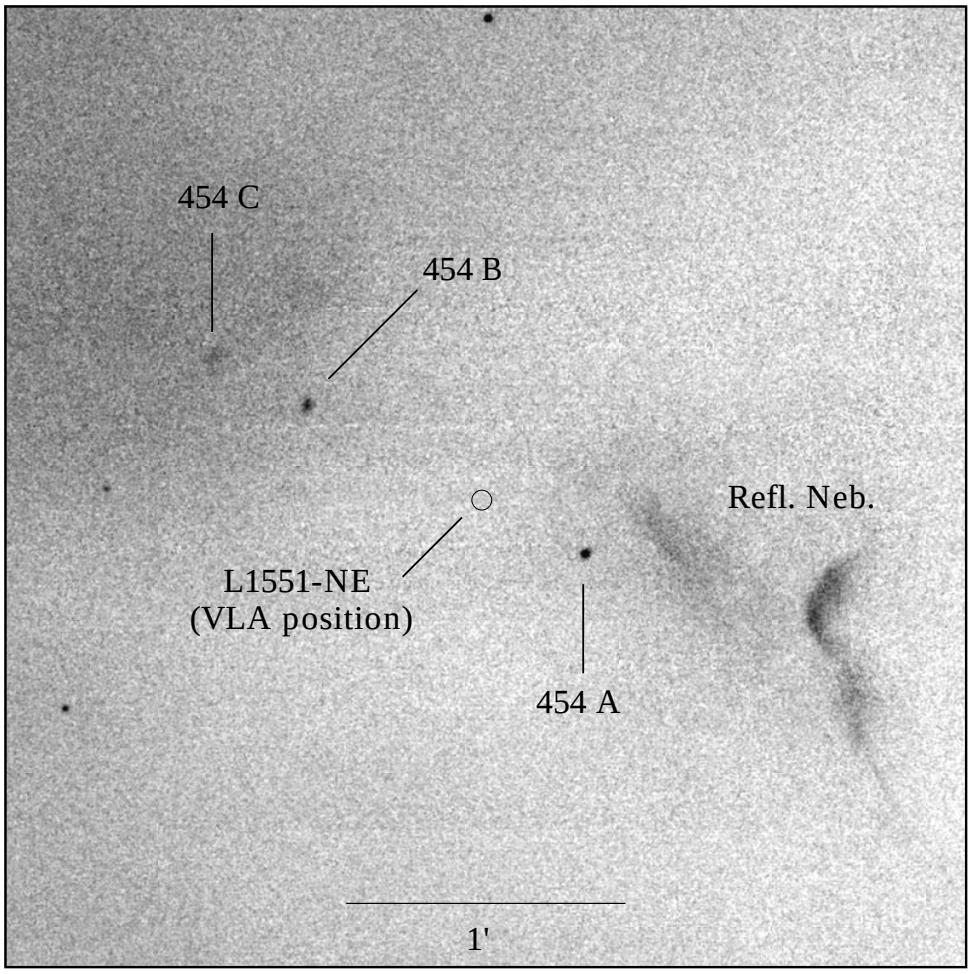

FIG. 3.—CCD image through an [S II] filter showing the HH 454 flow around L1551 NE

than 10′ away (see Table 1). These alignments are remarkable and strongly suggest that HH 454, the [Fe II] jet, and HH 28 and 29 all form part of one and the same HH flow, with a single lobe 0.7 pc in extent.

2. The morphology of HH 29 suggests that it is a bow shock, with wings swept backward as seen in Figure 4. The axis of symmetry is clearly better aligned with the direction to NE than to IRS 5.

These two arguments are just morphological, and a crucial test comes from the kinematics of HH 28 and 29. The compact infrared reflection nebula seen close to the NE source by Reipurth et al. (1999) opens up on the southeastern side of the source, suggesting that the radial velocities of HH 28 and 29 should be blueshifted relative to the L1551 cloud, and indeed they are (e.g., Stocke et al. 1988). In the following we discuss the proper motions of HH 28 and 29.

3.2. *New Proper Motions*

We measured proper motions in HH 29, in portions of HH 28, and in several emission-line structures between HH 28 and 29 that lie on the HH 454 outflow axis. This analysis was based on the NTT and KPNO images, which were obtained slightly more than 7 yr apart (only part of HH 28 was included in the NTT images). The NTT and KPNO images were matched in intensity, orientation, and plate scale based on common field stars following the procedure outlined in Heathcote & Reipurth (1992), and the proper motions were then determined using a code developed by Jon Morse and Pat Hartigan, based on a difference-squared cross-correlation algorithm described by Currie et al. (1996). The results of our proper-motion measurements are shown in Figure 5 and are summarized in Table 2. There are some obvious differences between the proper motions determined from the Hα and [S II] images, especially for some of the HH 28 and HH 259 knots. The source of these apparent disagreements does not appear to be due to a rotation or offset between images and is most likely related to differences between the physical regions traced by [S II] and Hα emission.

The proper motions listed in Table 2 were computed by cross-correlating the contents of a small square-shaped subimage extracted from the first-epoch image (centered on the coordinates listed in Table 2) with another slightly larger subimage extracted from the second-epoch image obtained in the same filter (Hα or [S II]). In complex fields such as L1551, it is important to isolate individual features as much as possible and prevent objects from crossing the boundaries of the cross-correlation box. Therefore, several box dimensions were used to extract proper motions. First-epoch box widths of either 11 or 21 pixels (4″.8 or 9″.2) were inflated to diameters of 17, 27, or 37 pixels (7″.5, 11″.9, or 16″.3) for extraction of the second-epoch images. (The first-

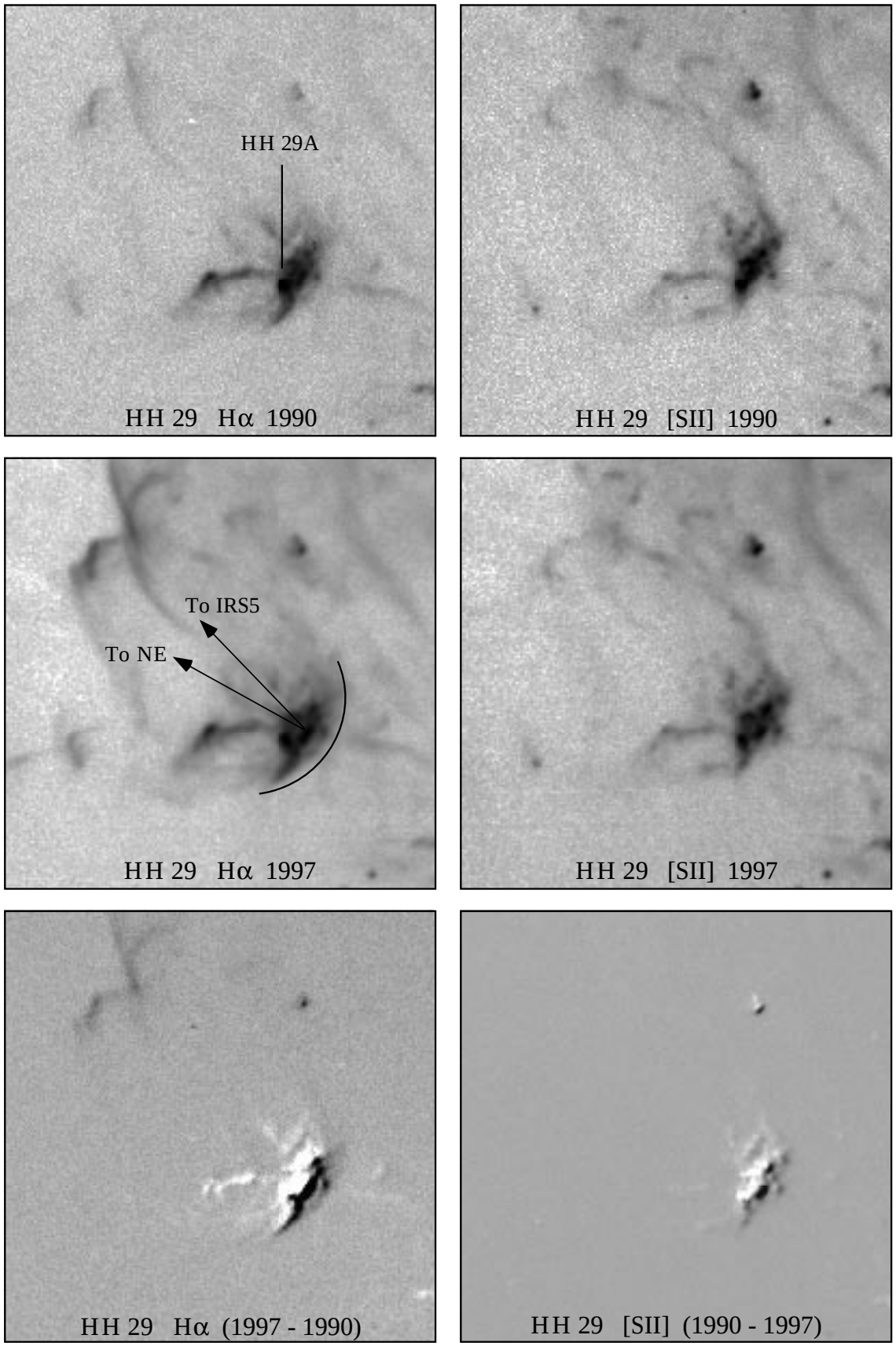

FIG. 4.—Structure of HH 29. *Top left*: A gray-scale Hα image (epoch 1990) shown with a logarithmic intensity scale. *Middle left*: An Hα emission-line image of the same region as it appeared in 1997. *Bottom left*: The Hα difference image (1997–1990), shown with black corresponding to 1997 and white corresponding to 1990. *Top right*: A gray-scale [S II] image (epoch 1990) shown with a logarithmic intensity scale. *Middle right*: An [S II] emission-line image of the same region as it appeared in 1997. *Bottom right*: The [S II] difference image (1997–1990), shown with black corresponding to 1997 and white correponding to 1990.

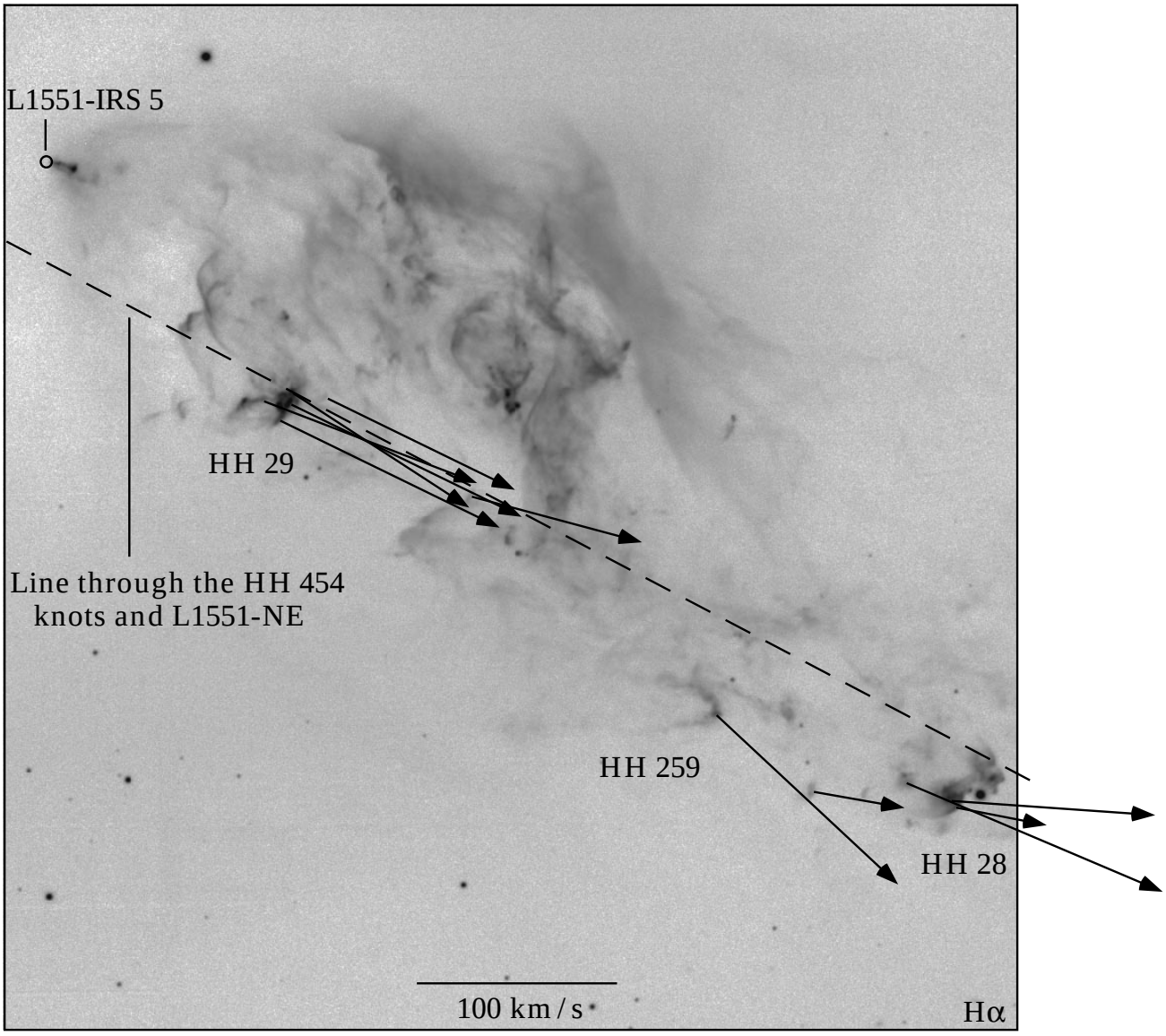

FIG. 5.—Proper-motion vectors for select Hα and [S II] knots in HH 29, HH 259, and HH 28 (see text for details)

epoch 21 pixel box was expanded to either 27 or 37 pixels in the second epoch). The second-epoch dimensions of the cross-correlation boxes are listed in the last column of Table 2.

We measured the proper motions of the brightest and most-isolated [S II] and Hα features along the NE outflow axis. Although some portions of HH 28 appear to be moving almost exactly along the HH 454 flow axis, others move along a direction pointing away from IRS 5. Since the projected angular separation between IRS 5 and NE is small from this remote location in the L1551 complex, the uncertainties in the measurement of the proper-motion vectors make it impossible to determine which is a more plausible driving source for the HH 28 complex based on the proper-motion data alone.

About a half-dozen compact bow-shaped emission regions and knots, collectively referred to as HH 259, lie between HH 28 and 29 on the HH 454 axis. As shown in Table 2, most of these features appear to be moving more to the west than to the south along a direction that indicates a point of origin close to L1551 NE and not near IRS 5. The bright knot embedded in the westward-facing bow (HH 259) two-thirds of the way from HH 29 to HH 28 appears to be moving almost exactly along the HH 454 axis in the [S II] images; however, the Hα images show a proper motion directed away from the general vicinity of IRS 5.

HH 29, which lies roughly midway between HH 28 and NE along the HH 454 flow axis, is a complex object, consisting of a cluster of bright clumps concentrated at the southwestern (leading) edge of a bow-shaped envelope that sweeps back toward NE. The brightest clump, HH 29A, is located several arcseconds to the northeast of the leading edge of HH 29. When the entire HH 29 complex is included in the cross-correlation box, the measured proper motion agrees with the results of Cudworth & Herbig (1979). Since we are arguing that the source of HH 29 is NE, and not IRS 5, we must explain this apparent contradiction. Table 2 lists measurements at various locations in HH 29, which exclude the emission from HH 29A, the brightest portion of HH 29, discussed further below. The Hα proper-motion determinations for these subregions point to motion away from NE rather than IRS 5. However, this result is more evident in

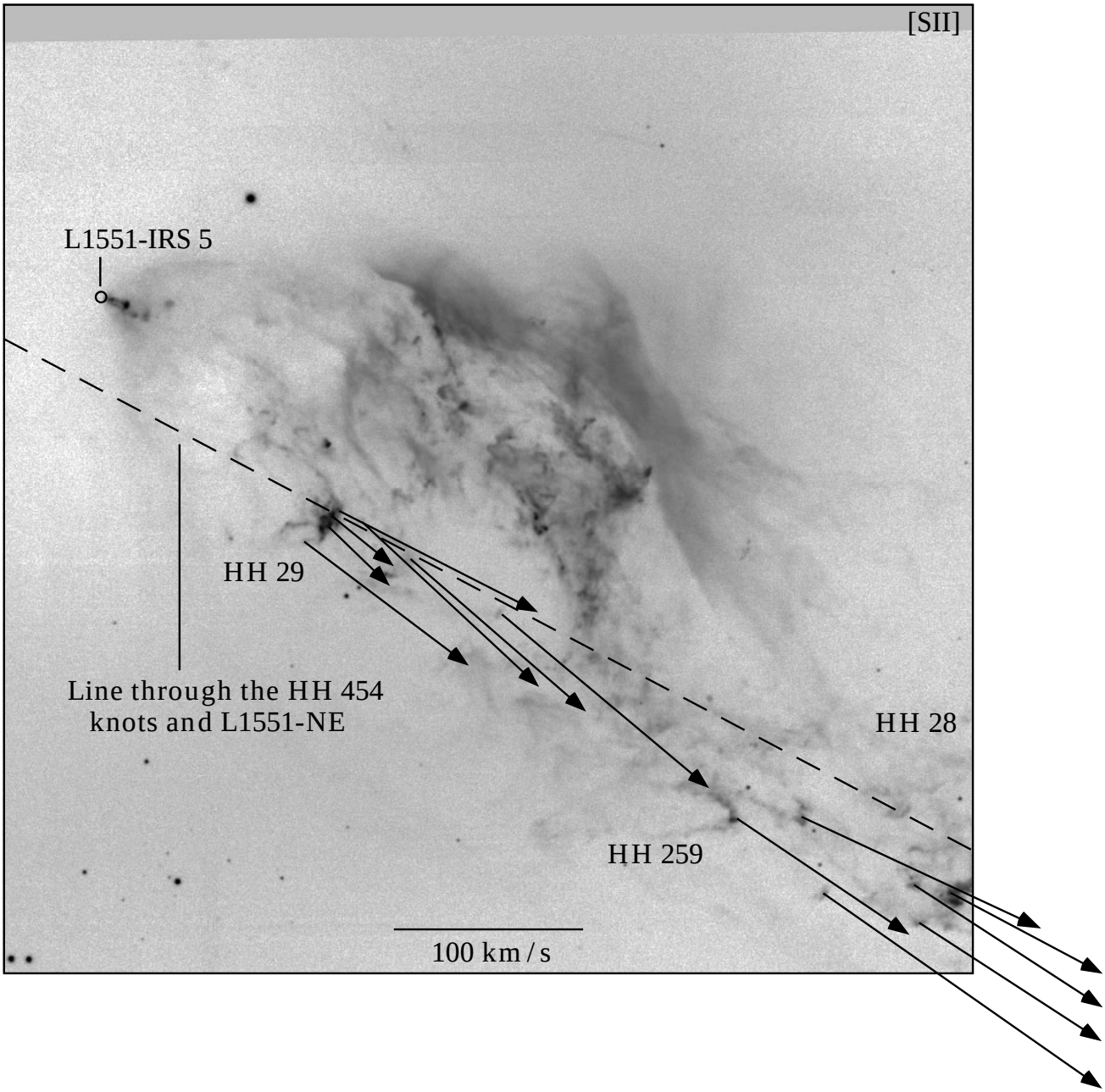

FIG. 5.—*Continued*

Hα than in [S II]. For one [S II] knot, the vector clearly points away from NE, but for the others, the results are ambiguous and the motion could be either from NE or IRS 5.

As shown in Figures 4 and 6, the morphology of the Hα emission associated with HH 29 has changed since 1990. The emission slightly northwest of HH 29A that is visible in the 1990 image has mostly disappeared by 1997, while the emission slightly west of HH 29A has brightened considerably. HH 29A itself appears roughly circular in the 1990 image but extends toward the southwest in the 1997 image along the direction of the apparent proper motions. Inspection of the 1990 and 1997 images reveals that HH 29A has a nearly stationary component that has faded since 1990; this is consistent with Fabry-Perot images of the region that show a much lower radial velocity for HH 29A than for the surrounding emission (Hartigan et al. 1999). Long-term *IUE* monitoring of HH 29 shows variability on timescales of less than 6 months (Liseau et al. 1995); hence, it seems likely that knot A is nearly stationary and highly variable and these variations in emission could have skewed the proper-motion measurements sufficiently to account for the apparent motion of HH 29 away from IRS 5.

The lower proper motion and radial velocity of knot A indicates that it is either a slower moving or a stationary clump that has been run over by a bow shock several decades ago. The impact of the bow shock would abruptly heat the clump, which would then cool and produce variable emission-line features. Fridlund, Liseau, & Gullbring (1998) concluded, on the basis of spectra and images, that HH 29 consists of a mixture of moving material and clumpy ambient material, and, in particular, they identify the very

TABLE 1

POSITIONS AND DISTANCES OF FLOW COMPONENTS RELATIVE TO L1551 NE

Object	α (2000)	δ (2000)	d (arcsec)[a]	D (pc)[b]	P.A. (NE)[c]	P.A. (IRS 5)[d]
L1551 NE[e]	04 31 44.44	+18 08 32.0	...	...	...	...
HH 454A[f]	04 31 42.7	+18 08 19	+28	0.02	242	254
HH 454B	04 31 46.9	+18 08 51	−39	0.03	242	256
HH 454C	04 31 48.3	+18 09 02	−62	0.04	242	263
HH 29.....	04 31 26.9	+18 06 17	+283	0.19	242	224
HH 28.....	04 31 06.7	+18 03 20	+620	0.42	240	234
HH 286	04 32 41.7	+18 16 36	−945	0.64	239	242

NOTE.—Units of right ascension are hours, minutes, and seconds, and units of declination are degrees, arcminutes, and arcseconds.

[a] The angular offset from L1551 NE. A plus sign indicates a location southwest of the source, and a minus sign a location to the northeast.

[b] Projected distance from L1551 NE, assuming a distance of 140 pc.

[c] The position angle relative to L1551 NE.

[d] The position angle relative to IRS 5.

[e] The radio continuum position of L1551 NE is from Rodríguez et al. 1995 and has been precessed to J2000 coordinates.

[f] The HH coordinates are for the brightest knot visible in the 1997 images and have a positional uncertainty of about ∼1″.

high excitation knot A as one of the stationary clumps, a result that is consistent with our observations. It is clear when blinking the first- and second-epoch images that knot A (and several other minor knots) is nearly stationary, while the rest of the bow-shaped HH 29 is rapidly moving past them. Thus the proper motions measured in regions containing all of HH 29 are likely to be seriously compromised by changes in its structure. Cudworth & Herbig

TABLE 2

PROPER MOTIONS FOR SELECT HH OBJECTS

Object	α[a]	δ[b]	V_E[c]	V_N[c]	P.A. (V)[d]	P.A. (NE)[e]	Species[f]
HH 28	12.5	17 56 55	−45	−8	259	241	Hα, 37
HH 28	12.7	17 57 01	−81	−42	242	241	[S II], 37
HH 28	12.8	17 56 57	−102	−7	266	241	Hα, 37
HH 28	13.8	17 56 45	−97	−62	237	240	[S II], 37
HH 28	14.0	17 57 06	−100	−65	237	240	[S II], 37
HH 28	13.8	17 57 04	−128	−53	247	240	Hα, 37
HH 28	17.0	17 56 59	−148	−102	235	238	[S II], 37
HH 28	17.0	17 56 59	−45	−8	260	240	Hα, 27
HH 259.....	17.6	17 57 34	−126	−59	245	240	[S II], 37
HH 259.....	19.9	17 57 34	−91	−62	236	239	[S II], 17
HH 259.....	19.9	17 57 34	−91	−84	227	238	Hα, 17
HH 259.....	27.2	17 59 14	−85	−22	255	243	Hα, 17
HH 259.....	27.5	17 59 12	−109	−92	230	242	[S II], 17
HH 259.....	30.2	17 59 36	−93	−81	229	243	[S II], 17
HH 29	31.8	17 59 57	−93	−46	244	244	Hα, 27
HH 29	31.9	17 59 56	−96	−85	227	244	[S II], 27
HH 29	32.5	18 00 00	−105	−54	243	244	[S II], 27
HH 29	32.5	17 59 53	−115	−56	244	243	Hα, 37
HH 29	32.7	17 59 54	−33	−26	231	243	[S II], 27
HH 29	32.8	17 59 57	−88	−57	237	243	Hα, 17
HH 29	32.9	17 18 04	−33	−31	226	244	[S II], 27
HH 29	33.2	17 59 46	−107	−59	244	241	Hα, 37
HH 29	33.7	17 59 46	−87	−65	233	240	[S II], 27
HH 29	33.7	17 59 55	−107	−40	249	242	Hα, 27

[a] Seconds of 1950 right ascension. Add the listed values to $04^h28^m00^s$.

[b] The 1950 declination.

[c] The components of the proper-motion vectors along east and north in km s^{-1}.

[d] The position angle of the proper-motion vector.

[e] The position angle of the HH object with respect to L1551 NE.

[f] The species (Hα or [S II]) and a code for the size of the box used to measure the proper motion with the quoted value being the number of 0.″4396 pixels in the second-epoch image. Code 17 implies that an 11 pixel first-epoch box was inflated to 17 pixels in the second epoch. Code 27 implies that a 21 pixel first-epoch box was inflated to 27 pixels in the second epoch. Code 37 implies that a 21 pixel first-epoch box was inflated to 37 pixels in the second epoch.

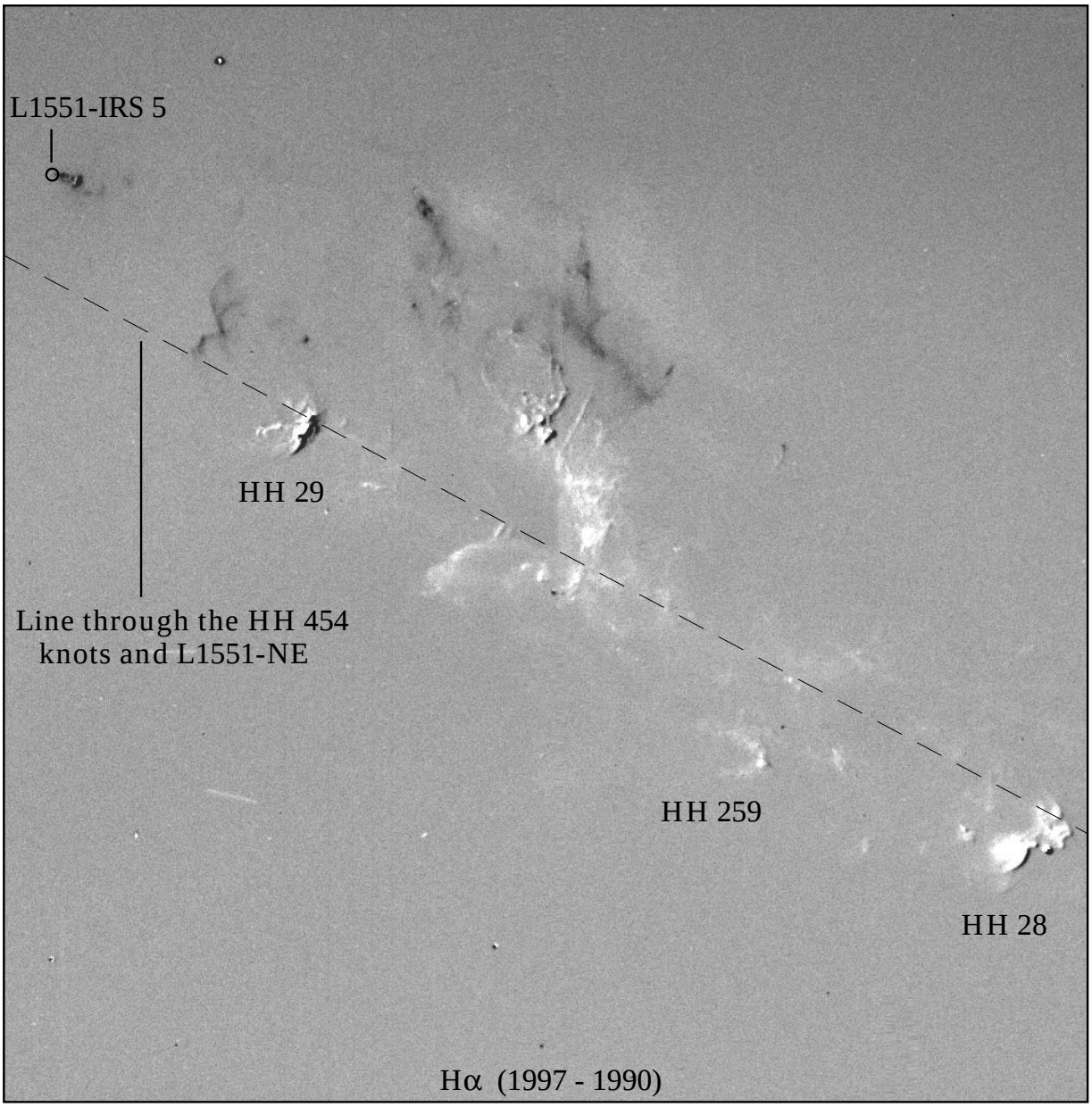

FIG. 6.—Gray-scale representation of the difference between the 1990 and 1997 Hα images. Black represents 1997 images, and white 1990 images.

(1979), in fact, mentioned the possibility of changes in the morphology of the southeastern portion of HH 29 in their Crossley plates of the region and suggested that future monitoring was in order.

The time variability of knot A offers a unique opportunity to study how a neutral globule is shocked and subsequently cools when hit by a passing shock wave, and photometric monitoring is therefore important. In this context, we note that the otherwise fairly smooth bow shock of HH 29 has a small gap right on a line through NE and knot A, strongly suggesting that it represents a wake or shadow formed as the bow shock overran the neutral globule, which then shocked and is now rapidly cooling. The direction of this shadow along a line to NE provides yet further support for an origin of HH 29 in this source.

Figures 6 and 7 and the lower panels of Figure 4 show the difference images produced by subtracting the initial 1990 image and the later 1997 image. The axis of the HH 454 flow that passes through NE is also shown. The stationary knot A is not fully subtracted because of its dramatic fading in the intervening 7 yr, while the bow shock of HH 29 has moved considerably along the axis from NE.

After combining all the above results (alignment of various features, structural symmetry of HH 29, and proper motions), it appears that the more deeply embedded source L1551 NE is a better candidate than IRS 5 for the driving source of the well-collimated HH 28/29 flow.

3.3. *HH Objects in the Red Lobe of L1551 NE*

We have discovered a new HH object (HH 286) approximately 945″ (0.65 pc) northeast of L1551 NE. HH 286 has the appearance of a partial bow shock and is more evident in Hα than in [S II]. The Hα emission has a smooth, arcuate appearance and is offset by 10″–15″ from the [S II] emission,

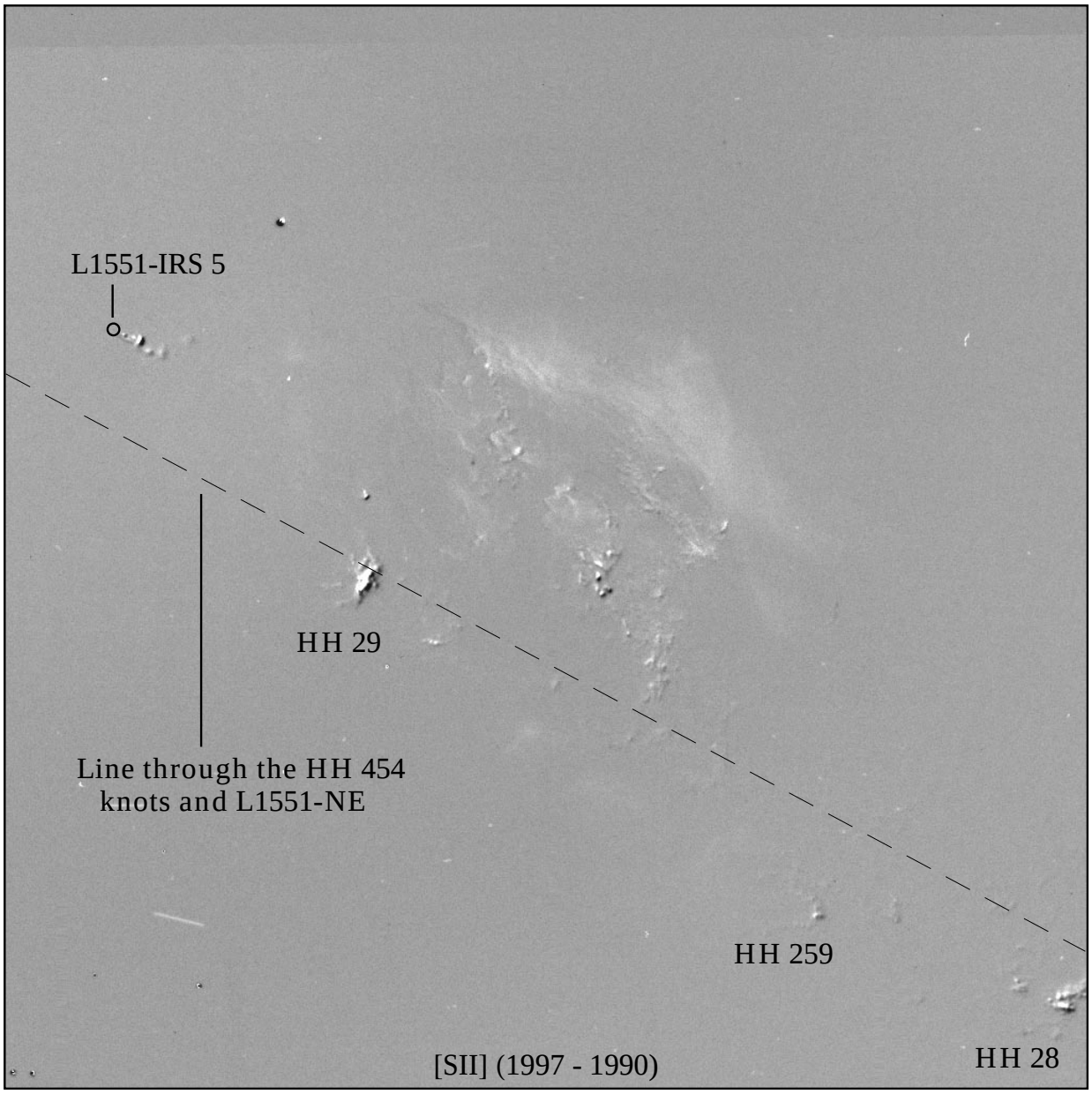

FIG. 7.—A gray-scale representation of the difference between the 1990 and 1997 [S II] images. Black represents 1997 images, and white 1990 images.

which is mostly concentrated in a small patch near the apparent apex of the bow shock. A long-slit spectrum of HH 286 shows redshifted emission peaked at roughly 80 km s^{-1} relative to NE and with a velocity dispersion of order 80 km s^{-1}. It is not clear if HH 286 is driven by L1551 NE or IRS 5. The apparent apex of HH 286 lies within 3° of the HH 454 flow axis; however, it is interesting to note that a line drawn from the apparent apex of HH 286 toward the southwest to the brightest knot in the HH 258 complex passes very close to IRS 5 (see Fig. 2). Numerous galaxies are visible in the region near HH 286, suggesting that the associated outflow must have punched clear of the surrounding molecular cloud into a region of very low extinction.

The HH 262 complex lies roughly midway between HH 286 and the L1551 NE and IRS 5 protostars. HH 262 is redshifted relative to IRS 5 (and NE) by between 0 and 90 km s^{-1} (Graham & Heyer 1990; Graham & Rubin 1992) and has proper motions of order 180 km s^{-1} with position angles ranging from $-25°$ to 146° (López et al. 1998). The wide range of position angles could be due to the presence of overlapping flows or to emission pattern changes in the HH knots. A few of the knots (GH25, GH18) have proper motions directed away from the general direction of L1551 NE and IRS 5, while others (GH10E-W, GH19, GH21) appear to be moving away from the HL-Tau region and are probably associated with the outflow HH 153 shown in Figure 1. A line drawn along the HH 454 flow axis points slightly south of HH 286 and HH 262, thus it is not clear whether these HH objects are associated with the NE flow or the IRS 5 flow. It is interesting to note that a line from NE toward HH 286 passes through the eastern edge of HH 262; thus, it is possible that several of the knots (especially those that we have labeled 262E) may be associ-

ated with the red lobe of the L1551 NE flow. Future proper-motion studies should be able to determine whether this is so.

4. CONCLUSIONS

Based on our wide field-of-view observations of the L1551 region and Hα images taken with a time difference of 7 yr, we have obtained the following results:

1. L1551 NE is driving an HH flow (HH 454) with the blueshifted lobe oriented toward the southwest. The flow axis determined by the [S II] bright HH 454 knots lies within 2° of the [Fe II] jet driven by NE (Reipurth et al. 1999). HH 454 exhibits kinematic bipolarity about L1551 NE with blueshifted emission extending toward the southwest and redshifted emission extending toward the northeast.

2. The well-known HH objects HH 29 and 28 lie almost exactly along the axis of the HH 454 outflow at distances of roughly 5′ and 10′, respectively, from NE. HH 29 has the appearance of a bow shock opening away from NE, as do portions of HH 28. In the opposite lobe, we find a new, distant counter bow shock, HH 286, but it is unclear if this is driven by NE or by IRS 5.

3. The structure and intensity of the Hα emission from HH 29 has changed considerably since 1990. HH 29 appears to be tracing the collision between several stationary clumps of material and a bow shock that is most likely driven by NE.

4. Some parts of HH 28 appear to be moving away from NE, while others have proper motions that appear to favor an origin in IRS 5, but the uncertainty of the proper motions and the closeness of NE and IRS 5 as seen from HH 28 make firm conclusions difficult. For HH 29, on the other hand, the proper-motion vectors taken at face value appear to point away from IRS 5. However, we argue that this apparent motion is due to a change in the emission pattern and to the presence of stationary knots associated with HH 29 and does *not* imply that HH 29 is driven by IRS 5. Detailed analysis of individual features in HH 29 shows that when stationary knots are disregarded, the bow shock–shaped part of HH 29 indeed has proper motions directed away from NE, not from IRS 5.

5. Combining these points leads us to suggest that HH 28 and 29 are most likely driven by L1551 NE, and not by IRS 5.

We thank Steve Heathcote for discussions and the staff at KPNO for their support while using MOSAIC.

REFERENCES

Armandroff, T., et al. 1999, NOAO CCD MOSAIC Imager User Manual (KPNO System) (Tucson, AZ: NOAO)
Bally, J., et al. 2000, in preparation
Barsony, M., & Chandler, C. J. 1993, ApJ, 406, L71
Campbell, B., Persson, S. E., Strom, S. E., & Grasdalen, G. L. 1988, AJ, 95, 1173
Cudworth, K. M., & Herbig, G. H. 1979, AJ, 84, 548
Currie, D. G., et al. 1996, AJ, 112, 1115
Davis, C. J., Mundt, R., Eislöffel, J., & Ray, T. P. 1995, AJ, 110, 766
Draper, P. W., Warren-Smith, R. F., & Scarrott, S. M. 1985, MNRAS, 216, 7P
Emerson, J. P., Harris, S., Jennings, R. E., Beichman, C. A., Baud, B., Beintema, D. A., Marsden, P. L., & Wesselius, P. R. 1984, ApJ, 278, L49
Fridlund, C. V. M., Liseau, R., & Gullbring, E. 1998, A&A, 330, 327
Graham, J. A., & Heyer, M. H. 1990, PASP, 102, 972
Graham, J. A., & Rubin, V. C. 1992, PASP, 104, 730
Hartigan, P., et al. 1999, in preparation
Heathcote, S., & Reipurth, B. 1992, AJ, 104, 2193
Herbig, G. H. 1974, Lick Obs. Bull. 658
Hodapp, K.-W. 1994, ApJS, 94, 615
Kenyon, S. J., Dobrzycka, D., & Hartmann, L. 1994, AJ, 108, 1872
Liseau, R., Huldtren, M., Fridlund, C. V. M., & Cameron, M. 1995, A&A, 306, 255
López, R., et al. 1998, AJ, 116, 845
Lynds, B. T. 1962, ApJS 7, 1
Massey, P., Valdes, F., & Barnes, J. 1992, A User's Guide to Reducing Slit Spectra with IRAF (Tucson, AZ: NOAO)
Moriarty-Schieven, G. H., Butner, H. M., & Wannier, P. G. 1995, ApJ, 445, L55
Reipurth, B. 1999, A General Catalogue of Herbig-Haro Objects (2d ed; Boulder: Cent. Astrophys. Space Astron., Univ. Colorado)
Reipurth, B., et al. 1999, in preparation
Rodríguez, L. F., Anglada, G., & Raga, A. C. 1995, ApJ, 454, L149
Rodríguez, L. F., Cantó, J., Moreno, M. A., & López, J. A. 1989, Rev. Mexicana Astron. Astrofis., 17, 111
Snell, R. L., Loren, R. B., & Plambeck, R. L. 1980, ApJ, 239, L17
Stocke, J. T., Hartigan, P. M., Strom, S. E., Strom, K. M., Andersson, E. R., Hartmann, L. W., & Kenyon, S. J. 1988, ApJS, 68, 229
Strom, K. M., Strom, S. E., & Vrba, F. J. 1976, AJ, 81, 320